Accepted Manuscript

Characterisation of coastal counter-currents on the inner shelf of the Gulf of Cadiz

E. Garel, I. Laiz, T. Drago, P. Relvas

Please cite this article as: Garel, E., Laiz, I., Drago, T., Relvas, P., Characterisation of coastal counter-currents on the inner shelf of the Gulf of Cadiz, *Journal of Marine Systems* (2015), doi: 10.1016/j.jmarsys.2015.11.001

Characterisation of coastal counter-currents on the inner shelf of the Gulf of Cadiz

E. Garel[1,*], I. Laiz[2], T. Drago[3], P. Relvas[1]

[1] Centre for Marine Sciences (CCMAR), Algarve University, 8005- 139 Faro, Portugal

[2] Department of Applied Physics, Faculty of Marine Science and Environment, University of Cadiz, Campus Rio San Pedro, 11510, Puerto Real, Spain

[3] Instituto Português do Mar e da Atmosfera (IPMA, I.P.) 1749-077 Lisboa, and Institute Dom Luiz (IDL), FCUL, 1749-016 Lisboa

[*] Now at Centre for Marine and Environmental Sciences (CIMA), Algarve University, 8005- 139 Faro, Portugal

Corresponding author: Erwan Garel (egarel@ualg.pt)

Abstract

At the Gulf of Cadiz (GoC), poleward currents leaning along the coast alternate with coastal upwelling jets of opposite direction. Here the patterns of these coastal countercurrents (CCCs) are derived from ADCP data collected during 7 deployments at a single location on the inner shelf. The multiyear (2008-2014) time-series, constituting ~18 months of hourly records, are further analysed together with wind data from several sources representing local and basin-scale conditions. During one deployment, temperature sensors were also installed near the mooring site to examine the vertical thermal stratification associated with periods of poleward flow. These observations indicate that the coastal circulation is mainly alongshore and barotropic. However, a baroclinic flow is often observed shortly at the time of flow inversion to poleward. CCCs develop all year-round and exclusively control the occurrence of warm coastal water during the upwelling season. On average, one poleward flow lasting 3 days was observed every week, corresponding to CCCs during ~40% of the time without seasonal variability. Thus, the studied region is distinct from typical upwelling systems where equatorward coastal upwelling jets largely predominate. CCCs often start to develop near the bed and are frequently associated with 2-layer cross-shore flows characteristic of downwelling conditions (offshore near the bed). In general, the action of alongshore wind stress alone does not justify the development of CCCs. The coastal circulation is best correlated and shows the highest coherence with south-eastward wind in the basin that proceed from the rotation of southward wind at the West coast of Portugal, hence suggesting a dominant control of large-scale wind conditions. In agreement, wavelet analyses indicate that CCCs are best correlated with alongshore wind occurring in a band period characteristic of the upwelling system (8-32 days). Furthermore, in the absence of wind coastal currents tend to be poleward during summer. This set of observations supports that CCCs develop in response to the unbalance of an alongshore pressure gradient during the relaxation of (system-scale) upwelling-favourable winds, oriented south-eastward in the basin. The relaxation periods defined based on this wind direction show a good correspondence with the periods of poleward flow.

Keywords

Coastal countercurrents; Upwelling; Wind-driven currents; Shelf dynamics; Relaxation; South-west Iberia; Gulf of Cadiz.

Highlights

- Coastal counter currents (CCCs) in the Gulf of Cadiz are characterised;
- CCCs occur frequently all-year round without seasonality;
- CCCs are barotropic (except at inversions) often with baroclinic cross-shore flows;
- Alongshore wind stress alone fails to justify the development of CCCs;
- CCCs relate to large-scale upwelling-favourable wind blowing south-eastward.

1. Introduction

Poleward currents leaning along the coast are characteristic features of Eastern Boundary Upwelling Systems (EBUS). These flows alternate with the predominant coastal upwelling jets of opposite equatorward direction, and are as such commonly referred to as "coastal countercurrents" (CCCs). The occurrence of CCCs has been reported in major coastal upwelling systems, in particular along the Gulf of Cadiz (GoC, Southern Iberia) in the Portuguese-Canary Current upwelling system (Mittelstaedt, 1991; Pelegrí et al., 2005a; Pelegrí et al., 2005b; Relvas and Barton, 2002), over the Namaqua shelf (South Africa) in the Benguela Current upwelling system (Fawcett et al., 2008), and in the northern (Kosro, 2005; Largier et al., 1993; Lentz and Chapman, 1989; Send et al., 1987; Winant et al., 1987), central (Harms and Winant, 1998; Melton et al., 2009; Washburn et al., 2011; Woodson et al., 2009) and southern (Dever, 2004; Winant et al., 1999; Winant et al., 2003) portions of the California Current upwelling system. Typically, 10 to 30 km-wide CCCs advect warm water previously retained in the lee of capes or embayments during active upwelling and temporarily displace the previously upwelled colder water offshore (Send et al., 1987). This process causes rapid temperature changes over the inner shelf (Melton et al., 2009; Relvas and Barton, 2002). In addition, CCCs may affect ecosystems with the transport of water-borne material such as pollutant and larvae into nearshore areas, where many subtidal and intertidal species settle (e.g., Dudas et al., 2008; Mace and Morgan, 2006; Wilson et al., 2008; Wing et al., 1995).

Most of the studies about the characteristics and forcing mechanisms of CCCs have been conducted at the California Current upwelling system, based on very extensive sets of hydrographic observations across and along the inner shelf, completed with wind data from buoys and coastal stations. Examples include the CODE experiments and the multiyear Santa Barbara Coastal Long-Term Ecological Research (SBCLTER) project (Melton et al., 2009; Washburn et al., 2011). A major result from these observations was the establishment that CCCs are driven by poleward alongshore pressure gradients (APGs) that result from differences in sea level along the coast. Large scale alongshore sea surface slopes are

produced between coastal headlands by the persistence of equatorward (upwelling favourable) winds (Largier et al., 1993; Winant et al., 1987; Winant et al., 2003). Numerical studies have further indicated that interactions between coastal upwelling jets and alongshore variations in the coastline and shelf bathymetry promote the development of smaller scale poleward APGs in the lee (i.e., equatorward) of capes and promontories (Gan and Allen, 2002). CCCs are triggered when these large- or small- scale APGs become unbalanced during wind relaxation events; these are defined as the weakening or even reversal of usually strong upwelling favourable winds (Huyer and Kosro, 1987).

In contrast with the Californian inner shelf, few studies have been devoted to the coastal circulation in the GoC. Until now, most of these works dealt with remotely sensed sea-surface temperature (SST) or climatological data (Fiúza, 1983; Fiúza et al., 1982; Folkard et al., 1997; Sánchez and Relvas, 2003; Vargas et al., 2003). The few hydrodynamic observations performed on the inner shelf with fixed stations (Lobo et al., 2004; Sánchez et al., 2006) or shipboard surveys (García-Lafuente et al., 2006) were of short duration (less than 1 month), with the exception of a multiyear (2002, 2004, 2005) current time-series used to examine the surface circulation at the seasonal and inter-annual time-scales (Criado-Aldeanueva et al., 2009). However, there is so far no detailed study based on long-term observations dealing with current inversions at an "event scale" for the definition of the patterns of poleward flows (e.g., duration and frequency) and their relation with wind conditions. Consequently, the CCCs patterns in this region and their driving processes are not clear yet. Based on SST satellite imagery, coastal wind and tidal gauges data, Relvas and Barton (2002) proposed that CCCs are driven by a background APG, similar to the situation along the Californian coast. Other processes that have been proposed for the production of an APG in southern Iberia include exchanges through the Strait of Gibraltar (Mauritzen et al., 2001), the effects of large-scale atmospheric pressure systems (Sánchez et al., 2006), and tidal advection of warmer (hence lighter) coastal water from the numerous shallow inland areas located in the Eastern GoC (García-Lafuente et al., 2006). Numerical studies also suggest that CCCs are produced in response to the action of wind stress alone, rather than to the relaxation of upwelling favourable wind (Teles-Machado et al., 2007). This latter hypothesis does not require a background APG for the development of CCCs.

The present research compiles 7 Acoustic Doppler Current Meter (ADCP) deployments of about 1 to 3 months duration at a single location on the inner shelf of the GoC. This dataset is used to characterise the dynamics of CCCs from an Eulerian perspective, with the aim of contributing to untangle the mechanisms that drive these currents in the region, including their connection with the offshore circulation. In particular, it is verified whether the action of wind stress alone is able to account for the observed periods of poleward flows.

2. Region of study

The GoC is the wide embayment of the Atlantic Ocean that constitutes the equatorward extremity of the Iberian upwelling system. The northern margin of the GoC stretches along the south-western Iberian Peninsula from Cape St Vicente (CSV, southwest Portugal) to the western side of the Strait of Gibraltar (Figure 1). Cape Santa Maria (CSM) divides the continental shelf (approximately bounded by the 150 m isobath) into two halves with distinct morphological settings. West of CSM the shelf is narrow (< 15 km) and incised with various canyons; to the East, it is steep and narrow (< 5 km) near CSM, but quickly widens (> 40 km) eastward with a gentle slope. These characteristics may create a distinct and independent water circulation over the eastern and western regions (Criado-Aldeanueva et al., 2009; García-Lafuente et al., 2006).

The upwelling season of the Iberian upwelling system is well-defined between April and October (Fiúza et al., 1982; Haynes et al., 1993; Peliz and Fiuza, 1999; Wooster et al., 1976), based on highly contrasted seasonal wind regimes associated with the zonal displacement of the Azores high- and Icelandic low-pressure systems. During the upwelling season, strong northerly winds blow along the West coast, while westerlies and southwesterlies prevail in winter. Northerlies rotate counter clockwise around CSV and blow south-eastward off southern Portugal, due to the establishment of a low pressure centre over the Iberian Peninsula in summer, together with orographic constraints (Relvas and Barton, 2002).

Although included in the Canary Current Upwelling System (CCUS), the eastern boundary discontinuity imposed by the entrance to the Mediterranean Sea modifies the Canary Current upwelling regime prevailing at the GoC. Typically, the Iberian upwelling system is associated with equatorward coastal flows (i.e., southward and eastward along the West and South coasts, respectively) of cool water forced by geostrophic adjustment. East of CSV, however, the coastal jet proceeds from the one affecting the West coast, and its propagation along the South coast depends on the local wind conditions, with westerlies and easterlies promoting and hampering its poleward extension, respectively (Fiúza, 1983; Fiúza et al., 1982; Folkard et al., 1997; Sánchez and Relvas, 2003). Westerlies also tend to produce a secondary upwelling core immediately east of CSM that may merge with the more permanent core off CSV. Overall, while the upwelling regime is quasi-permanent in summer at the West coast, the intensity and occurrence of upwelling events at the South coast is significantly reduced, in particular towards the Eastern GoC, as reported by Relvas and Barton (2002) based on the analysis of a multiyear dataset of SST images. These data further show that the coastal circulation during summer along the South coast is rather dominated by the alternation of equatorward (i.e., eastward) upwelled water and a poleward (i.e., westward) warm flow (CCC) propagating from the eastern GoC. In their detailed study based on cloud-free satellite images available mostly during the summer months, Relvas and Barton (2002) have noted the presence of warm CCC during 45% of the time at the South coast. These flows were associated with temperature increases, reaching more than 5°C in some cases. The coastal tongue of warm water is typically about 10-15 km wide, with an estimated velocity around 0.2 m s^{-1} that has been confirmed by direct

measurements in summer (García-Lafuente et al., 2006) and winter (Sánchez et al., 2006). Based on cross-shore ship measurements, García-Lafuente et al. (2006) have suggested that the CCC is a stable feature in summer, being the northern boundary of a cyclonic cell located on the eastern shelf between CSM and the mouth of the Gualdalquivir Estuary (for location , see Figure 1). In any case, the propagation of poleward currents depends on local wind conditions (Fiúza, 1983; Folkard et al., 1997; Relvas and Barton, 2002). García-Lafuente et al. (2006) have further proposed that westward blowing wind is required for the coastal current to pass over CSM. In extreme cases, CCCs may reach CSV and extend more than 100 km northwards along the West coast (Relvas and Barton, 2002). SST images in winter also show the occurrence of CCCs associated with a cold water signature along the coast. The presence of a pool of cold water on the eastern GoC in winter has been attributed to freshwater advection from the large rivers of this coastal sector (Peliz et al., 2004).

3. Data and Methods

3.1. Data

Current velocities along the water column and near-bed temperature were collected with an Acoustic Doppler Current Profiler (ADCP Workhorse 600 kHz, TRDI). The instrument was bottom-mounted 7 times between 2008 and 2014 at a single location (37° 0.648' N; 7° 44,480' W) on the inner shelf of the GoC, at 23 m water depth east of CSM (Figure 1). The deployments were performed during various periods of the year and for durations ranging from 40 to 133 days (Table 1). The instrument was installed inside the upper part of an artificial reef at 1.40 m from the bed. Various instrument configurations were used for each deployment, as the main objective was not always the study of the coastal water circulation. Velocity ensembles were recorded within cells of 0.5 or 1 m in thickness, every 5 to 60 min. The uncertainty (standard deviation) of the measured velocities was generally less than 0.015 m s^{-1}. In total, the dataset contains 598 days of hourly records (Table 2). Observations were mostly performed from May to December (> 1,000 hr each month); they were comparatively fewer in January, February and April, and no data were collected in March (Table 2). Despite this uneven temporal distribution, the seasonal variability of poleward flows can be examined through the comparison of the months of June to August and of November to January. For these months, the summer and winter seasons are well-established, hence avoiding transitory months that may smooth the results of seasonal comparisons. In addition, a large and similar number of current observations are available for these 2 contrasted periods (see Table 2).

Hourly wind data were obtained from the Cadiz offshore buoy, located over the 450 m isobath at ~90 km from the mooring site (Figure 1). Due to its offshore location, this buoy is generally considered as representative of the wind conditions in the eastern GoC (Criado-Aldeanueva et al., 2009; Criado-Aldeanueva et al., 2006; García-Lafuente et al., 2006). In the present paper, wind direction follows the oceanographic convention (the wind direction is

where the wind is blowing) to ease comparisons of wind and current data. Wind conditions during the deployments were typical of the seasonal wind regime in the basin (Figure 2). In particular, while the wind velocity was mild and principally blowing south-eastward in June-August (Figure 2b), velocities were stronger with larger occurrences of westward to southward winds in November-January (Figure 2c).

Additional wind sources located near the mooring site were also considered to examine whether the local wind is more able to account for the development of CCCs than the basin-scale wind from the Cadiz buoy. These sources include (for location, see Figure 1): a coastal station (Tavira) providing observations every 10 to 30 min; a mesoscale atmospheric model of 15 km resolution (HIRLAM) with outputs at 1 to 3 hr intervals; and remotely-sensed wind from daily passes of a satellite scatterometer (ASCAT). Wind data at Tavira station were not available for deployments 6 and 7; likewise, ASCAT data for deployment 7.

A thermistor chain with 3 temperature-depth (TD) sensors (Star-Oddi, DST centi-TD) was deployed from the 5th of August to the 5th of November 2014 (i.e., spanning the entire Deployment 6), at ~100 m from the ADCP mooring site. The sensors were mounted along a rope fixed at the bottom and maintained vertical with a small surface buoy, providing hourly records at ~7 m, ~13 m and ~18 m water depths.

3.2. Processing

The ADCP data, collected at various time intervals, were ensemble averaged at a one hour interval. The cells located above 10% of the total pressure depth, and the cell immediately below, were discarded due to side lobe interferences at the surface boundary. Furthermore, cells having at least 3 of the 4 beams with a correlation magnitude less than 64 counts, and those having 2 or more beams with a vertical difference greater than 30 counts were invalidated. Ensembles with at least 1 invalidated cell were also discarded. Validated velocity data were then vertically interpolated every 50 cm at a range extending from 2.2 m from the ADP head (3.6 m from the bed) up to the last valid cell near the surface boundary. The east- and north-velocity components were rotated into along- and cross-shore components according to the angle of maximum variance. The latter was computed separately for each deployment to account for potential variability in the flow direction. The flow was however essentially parallel to the shore during the 7 deployments, ranging from 37°E (counter-clockwise from East, hereafter) to 31°E in 2010 and 2013, respectively. For each ensemble, depth-averaged velocities of the cross-shore and along-shore components were computed as the mean velocity.

Wind data from the Cadiz offshore buoy are measured at an elevation of 3 m from the sea surface; they were reduced to a height of 10 m using a power law profile with a Hellman exponent of 0.11 representing typical open water conditions. The data from the other wind sources were already measured or reduced at 10 m height. The Cadiz buoy was not

transmitting from the 6th of December 2014 to the 14th of March 2015. The corresponding data gap (at the end of deployment 7) was filled up with data from the HIRLAM model. For each deployment period, wind velocities were interpolated and rotated in along- and cross-shore components, using the same time (1 hr interval) and angles of variance than those considered for the ADCP data. The wind stress was then computed according to Large and Pond (1981).

In order to remove tidal and other higher frequency oscillations, all the (current, wind and temperature) time-series were low-passed filtered using a Butterworth filter with a 40h cut-off period. Every reference to the data hereafter applies to the low-pass filtered time-series, unless stated otherwise. Likewise, equatorward and poleward flows refer to depth-averaged alongshore currents oriented north-eastward and south-westward, respectively, along the studied coastal stretch. Similarly, poleward wind indicates alongshore wind blowing towards the western GoC. The term "inversion" is exclusively used to describe the reversal of alongshore flows from equatorward to poleward (i.e., the development of CCCs). CCC (or poleward flow) events refer to the periods when these flows are observed continuously. Finally, "winter" and "summer" strictly refer to the months of June-August and November-January, respectively (transitory months being the other months), except where indicated.

4. Observations of poleward flows

4.1. General CCC patterns

Alongshore current direction varies at a time scale of about 4 days, on average, at the mooring site (Figure 3a). Maximum equatorward and poleward values are up to ~0.4 m s^{-1}. The mean velocity of CCCs and equatorward flows was 0.12 m s^{-1} and 0.16 m s^{-1}, respectively. Both flows have a distinct signature: equatorward flows often stabilise near maximum values during few days before decreasing, outlining a rectangular-shaped positive curve; CCCs are characterised by short peaks of maximum velocities, resulting in a spiky negative velocity time-series. The maximum depth-averaged poleward current velocity of the non-filtered time-series was 0.52 m s^{-1} on the 11th of December 2013 (not shown).

CCCs are frequently observed (42% of the time), with no significant difference between the summer (41%) and winter months (43%; Table 2). In total, 82 current inversions were observed, with 4 and 3.3 inversions per month in summer and winter, respectively (Table 2). The longest CCC event lasted ~15 days, from the 23rd of November to the 8th of December 2013 (Figure 4a). In summer, the longest CCC event was ~9 days from the 29th of August to the 7th of September 2010. Overall, the mean duration of these events was 2.9 days, with no clear seasonal trend (3.4 and 3.2 days in winter and summer, respectively; Table2; see also red line in Figure 4a).

On average, CCCs were stronger in winter (0.09 m s^{-1}) than in summer (0.05 m s^{-1}) due to the occurrence of westward winter storms. An opposite pattern was observed for the mean

equatorward flow, being 0.07 m s^{-1} in summer and 0.03 m s^{-1} in winter. Peak CCC velocities were also generally larger in winter (in particular, in December) than in summer (see red line in Figure 4b). As an example, 39% of the CCC events in winter reached velocities > 0.25 m s^{-1}, but only 23% in summer. Yet, the maximum velocity of poleward flows may occasionally be as large in summer as in winter (Figure 4b). In fact, the largest velocity (0.41 m s^{-1}) of the entire time-series was on the 8th of August 2010 during an event lasting 8.5 days (Figure 3a; Figure 4b).

Overall, there is a broad positive correlation between the duration of the CCC events and the associated peak velocity (Figure 5), as pointed out by the similar variation of the monthly averaged lines in Figures 4a and 4b. A linear (or nearly linear) correlation is conspicuous for peak velocities < 0.2 m s^{-1} and duration < ~4 days. Generally, CCC events were long and strong in winter and summer, and short and weak during transitory months (Figure 5).

The cross-shore flow component is one order of magnitude lower than the alongshore component, rarely exceeding 0.04 m s^{-1} (Figure 3b). This confirms that the coastal circulation is essentially parallel to the coastline in the region. More specifically, the cross-shore flow is predominantly landward (71% of occurrence during the entire observation period), with no seasonal differences: landward flows were observed 69% and 67% of the time in summer and winter, respectively. Cross-shore flows were however more often onshore at the time of poleward flow (75%) than equatorward flows (67%). The development of CCCs is often associated with sharp peaks of offshore velocities up to ~0.05 m s^{-1}, such as on the 29th of April 2014 and 20th of November 2014 (Figure 3b). These peaks result from small veering clockwise of (still strong) alongshore current at the start of inversions.

4.2.   CCCs and temperature

Near bed temperatures from the ADCP varied between 13°C (30th of May 2014) and 23.5°C (16th of September 2010), exhibiting a strong seasonal variability (Figure 3c). During the non-upwelling season, the water temperature at the study site was less than 16°C and slowly varying, with the coldest value in February 2014 (13.15°C). During the upwelling season, the temperature was highly variable and ranged between 14°C and 24°C. The overall temperature pattern is consistent with the North Atlantic seasonal cycle, with the higher variability attributed to the occurrence of upwelling events.

During the upwelling season, the development of poleward (equatorward) flows was always associated with temperature increases (decreases), although sometimes small (e.g., < 1°C for the weakest events). The most pronounced temperature rise was 6°C in only 3 days, during a CCC event peaking up to 0.32 m s^{-1} (September 2010, Deployment 3 on Figure 3). Similar sharp temperature increases associated with strong CCC events were observed in

the summers of 2008 (Deployment 1) and 2014 (Deployment 5; Figure 3). Due to the advection of warm water by the poleward flow, the distribution of temperature is skewed toward higher values (Figure 6). Clearly, CCCs control the occurrence of warm water during the upwelling season. Considering only the summer months (June-August), a linear relation (dT = 12u_{max}) is found between the temperature increase (dT, computed as the difference between maximum and minimum temperature values) and peak velocity (u_{max}) during poleward flow events, with a correlation coefficient (r) of 0.89 (Figure 7).

During the non-upwelling season, CCCs are associated with small temperature changes (increase or decrease, if any), generally < 1°C (see for example December 2010 and 2014 on Figure 3) due to the homogenization of the temperature gradients during winter.

4.3. Vertical structure of CCCs during the thermistors deployment

Several current reversals were recorded during the thermistors deployment in summer 2014 (Figure 8a, where poleward flows are contoured in blue). As previously observed, all CCC events were associated with temperature increases (from < 1°C to > 5°C), with larger changes corresponding to stronger velocities. The arriving of warm water was accompanied with an increase of thermal stratification along the water column (Figure 8c). This is well-evidenced by the temperature records from the 2 sensors nearest to the bed, which differ only during poleward flow events (e.g., 19th to 22nd of August and 03rd of September in Figure 8). A 2-layer alongshore flow was often observed at the time of inversions with the flow reversal first occurring near the bed (see the leftward slope of the thick contour separating equatorward and poleward flows in Figure 8a). However, the temperature near the surface increased generally earlier than near the bed (Figure 8c). In some cases, the near surface temperature often started to increase while the flow was still equatorward (see the example denoted with arrows in Figure 8).

As noted previously (Figure 3b), inversions were associated with pulses of offshore flows due to small currents meanders, which were also observed during the thermistors deployment (see the dark blue areas in Figure 8b). The pulses appear along the entire water column, indicating that the flow veers barotropically. Once the CCCs had developed, a relatively vigorous 2-layer flow was generally established (during the temperature rise), with offshore velocity near the bed and onshore velocity near the surface, characteristic of downwelling conditions (Figure 8b). This is for example the case after the inversion indicated with an arrow or after the first inversion (7th of August) in Figure 8.

4.4. Alongshore wind stress and poleward flow

During the upwelling season, the alongshore wind stress at Cadiz buoy was low (generally < 0.05 N.m^{-2}) and predominantly eastward (Figure 3d). In contrast, the non-upwelling season was characterised with the frequent occurrence of gales in both the eastward and westward directions, while periods with weak wind stress (< 0.05 N.m^{-2}) rarely exceeded a week.

These differences in the alongshore wind stress reflect typical seasonal changes of wind regime in the basin. Indeed, during the non-upwelling season winds are not only stronger but also more parallel to the alongshore direction than during the upwelling season (see Figure 2). These seasonal patterns are not associated with similar variations in the magnitude of alongshore currents (Figure 3). Westward storms clearly correspond to large poleward flow velocities (e.g., November 2010) and to long CCC events (e.g., November 2013). Nevertheless, these relations are not always observed. For instance, no inversion was observed during the short gale of November 2008 with westward alongshore wind stress exceeding 0.2 N.m^{-2} (Figure 3).

The periods of poleward wind from various sources and poleward flow were plotted together along the time-axis to verify their overall temporal correspondence (Figure 9). The red horizontal lines represent the periods with poleward flows. These (red) lines are superimposed to thicker lines indicating the periods with poleward wind at the atmospheric model (HIRLAM, upper, blue), satellite observations (ASCAT, grey), the coastal station (Tavira, green) and the offshore buoy (Cadiz, blue). The lower (black) line denotes relaxation periods discussed in Section 5.4. At first glance, the red and thicker lines roughly correspond, indicating that CCCs generally occurred at approximately the same time as poleward wind at all the sources. The percentage of time with combined poleward flow (> 0.1 m s^{-1}) and poleward wind is also indicated in Figure 9. The percentage of time with combined poleward flow (> 0.1m/s) and poleward wind is also indicated in Figure 9. This percentage is largest for Cadiz and ASCAT (65%), followed by HIRLAM (62%); Tavira station shows a much lower score (50%). This confirms that it is reasonable to consider Cadiz buoy data as the most representative of the wind conditions affecting water circulation in the basin, in agreement with previous studies (Criado-Aldeanueva et al., 2009). Interestingly, HIRLAM and ASCAT data can also be useful, while coastal stations should be discarded most probably because of land effects. Looking into more details, the lag of CCC in relation to poleward wind (at Cadiz) was computed considering only the events that could be clearly identified (i.e., a single CCC event associated to a single poleward wind period) and with a maximum lag of 3 days (although the latter conditions did not affect the overall results). On average, inversions occurred 18 hours after the set up of poleward wind; likewise, flow reversal to equatorward occurred 23 hours after the wind (for example, see the events annotated 'lag' below Cadiz line in Figure 9). This indicates that alongshore flows reverse more easily from equatorward to poleward than the opposite in response to local or basin-scale wind. In addition, several CCC events were not associated with poleward wind at any source (see for example the events annotated 'x' in Figure 9). Inversely, numerous periods of westward wind at all the sources were not associated with poleward flows (for example, see the events annotated 'o' in Figure 9).

When looking at specific events, a good match was sometimes observed between CCCs and wind from all sources (e.g., October 2008 and November 2010 in Figure 10a, b). In these examples, the inversion lags the setup of poleward wind, as previously observed (e.g., 'lag'

in Figure 9). However, for a number of reversals, current and wind displayed markedly different patterns. In some cases, the inversion occurred before the wind from all sources blew poleward (for example, see 1st of December 2008, 23rd of November 2010 and 7th of December 2010 in Plate 1 provided as supplementary material). Furthermore, there were some relatively long periods with large poleward wind speeds at all sources which were not associated with CCCs but rather with a relatively strong equatorward flow (e.g., 22nd of January 2014 in Figure 10d; see also 26th of November 2008 and 23rd of January to 3rd of February 2014 in Plate 1). Inversely, inversions occurred while none of the winds from the distinct sources was blowing poleward (e.g., May 2008 in Figure 10c; see also 6th of November 2010, 30th of October 2010 and 22nd of June 2014 in Plate 1).

5. Discussion

5.1. Dynamics of CCCs

CCCs are common features of EBUS. Although they have been recognised in all major systems, they have been mostly characterised along the Californian coast (e.g., Send et al., 1987). Of particular interest is the Santa Barbara Channel (SBC), which shares similar coastline configuration with the GoC northern margin. The main geographical differences between both regions are the discontinuity imposed by the Strait of Gibraltar at the GoC and the existence of the Channel Islands at the SBC. CCCs velocities reported in the SBC are of similar order of magnitude than those documented here and in previous studies at the GoC (García-Lafuente et al., 2006; Sánchez et al., 2006). For example, Melton et al. (2009) reported poleward subtidal velocities of up to 0.5 m s^{-1}, corresponding to a propagation speed of 10-30 km day^{-1}. Similar velocities were also reported along the northern California shelf (Send et al., 1987). Poleward flows are observed all year-round at the GoC and SBC. However, CCCs may advect warm water in the winter season at the SBC but not at the GoC. This is probably because the GoC, contrarily to the SBC, has large rivers on the eastern side of the bight that discharge cold water during winter, particularly between November and March (Navarro and Ruiz, 2006).

While no seasonal pattern was identified at the GoC, CCCs are more frequent from March to November in the SBC and less frequent in December-January (Melton et al., 2009). This result at the SBC was obtained without considering inversions during winter storms, as the study focused on wind relaxation events. In contrast, the present study considered all periods of poleward flow for the general characterisation of these currents. With storms defined as events with alongshore wind velocities > 7 m s^{-1} (corresponding to a stress of 0.068 N.m^{-2}), about half of the inversions in winter occurred during storms, while no storms took place in summer. If winter storms are discarded, the number of inversions would therefore be larger in summer than in winter, as at the SBC. Note however that inversions occurring during winter storms might still develop primarily in response to a wind relaxation process.

Similar to the SBC, current inversions are mainly barotropic at the GoC, but tend to start near the bed (Figure 8). To examine the dynamics of these events, a principal component analysis (PCA) was applied to the alongshore velocity time series in order to separate the barotropic flow from the 2-layer baroclinic flow (see Garel and Ferreira, 2013; Stacey et al., 2001). The vertical structure of the flow was resolved using 25 cells ranging from 2.2 to 14.7 m from the bed, with a PC1 that was the barotropic velocity profile and a PC2 that was a 2-layer flow. Results are consistent between each deployment and are only shown for the thermistors deployment together with examples of the vertical alongshore flow structures of PC1 and PC2 at selected times (Figure 11, where CCC events are outlined with grey boxes). The PCA analysis confirms that the alongshore flow is largely barotropic, with PC1 defining 98.08 % of the total variance (Figure 11c and e), while PC2 defined almost all (1.74 %) the remaining variance. This is in agreement with the essentially unidirectional flow observed in Figure 8a. The examples (Figure 11f, g) are provided at times when PC2 is peaking, hence showing a well-developed baroclinic flow along with the barotropic component. Note however that these specific cases should not be considered as representative of the typical contribution of PC1 and PC2 to the overall variability. The largest peaks of energy (square of velocity) of PC1 often correspond to CCC events (Figure 11a), as poleward flows generally reach larger velocities than equatorward flows; this is related to the previously described "spiky" and "plateau-like" pattern of poleward and equatorward flows, respectively. PC2 energy is one order of magnitude lower than PC1 energy, and displays also commonly large peaks in association with poleward flows (Figure 11b). As observed previously (Figure 8a), these peaks occur predominantly - but not only - near the start and end of CCC events (Figure 11b) at times of strong current acceleration or deceleration. Considering the whole time series, the near-bed PC2 is poleward 50% of the time, and slightly more during poleward flows (54% of the time). Considering a time window of 4hr, centred on the time of current reversal, 62% of the near-bed PC2 is poleward at the start of CCC events, and only 29% at the end. This indicates that, very generally, the baroclinic flow tends to be equatorward near the surface and poleward near the bed during inversions; likewise, the flow is poleward near the surface and equatorward near the bed during the reversal to equatorward. Yet, the overall contribution of the baroclinic flow on the total flow is generally negligible, as illustrated by the high similarity between PC1 and the observed flow (Figure 11c, e). The baroclinic flow component may account for a significant part of the total flow only when the barotropic flow is very weak. Under these conditions, a 2-layer flow might develop, as observed in Figure 8 and exemplified in Figure 11g. Note that the latter example corresponds to the baroclinic events denoted with arrows in Figure 8.

At the SBC inner shelf (15 m water depth), the arrival of warm water is associated with the development of a 2-layer cross-shore flow directed onshore near the surface, typical of downwelling conditions (Melton et al., 2009). The alternation of upwelling-downwelling cycles allow onshore-offshore exchanges of nutrients and other water-borne material, and

are as such essential to support near-shore ecosystems (Washburn and McPhee-Shaw, 2013). In the present study, a 2-layer cross-shore flow was also observed during the thermistors deployment (Figure 8b), with blue areas (offshore flow) near the bed generally topped by red areas (onshore flow). This baroclinic flow was clearly stronger during CCC events (the darkest red and blue areas in Figure 8b correspond to poleward alongshore flow denoted in blue in Figure 8a). Hence, the previously described PCA method was applied to the cross-shore flow to analyse the development of the baroclinic and barotropic flows during CCC events. Like for the alongshore flow, the results are consistent between deployments and have only been represented at the time of the thermistors deployment (Figure 12). The dataset is dominated by PC1, which defined 67% of the variance; PC2 defined a large part (26%) of the remaining variance. Examples of the contributions of PC1 and PC2 to the measured profile are shown in Figures 11g and h. The largest peaks in energy of both PC1 and PC2 were associated with CCCs. The PC1 peaks correspond to the previously mentioned small veering of the alongshore flow at current inversions (e.g., Figure 12h, corresponding to the event annotated with arrows in Figure 8). PC2 energy peaked mostly during CCCs events (annotated with grey boxes in Figure 12). In details, the PC2 associated with poleward flows is mainly offshore near the bed (figure 12d), hence onshore near the surface, typical of downwelling conditions. Overall, offshore near-bed PC2 occurred 50% of the time considering the whole time series, but 70% of the time during CCC events. This set of observations indicates that poleward flows tend to be accompanied with the intensification of the cross-shore baroclinic circulation depicting predominantly downwelling conditions (e.g., Figure 12g). Further studies are required to study the effect of these flows on the exchanges between the coastal and open sea areas.

5.2. *Linkage between CCC and open sea circulation*

Previous studies at the GoC based on current observations have proposed that the shelf circulation is cyclonic in spring-summer and anticyclonic in autumn-winter due to strong coupling to the open sea circulation, the latter being forced by the seasonal wind regime in the basin (Criado-Aldeanueva et al., 2009; García-Lafuente et al., 2006). In this view, the inner shelf circulation is predominantly poleward in spring-summer, when wind blows mainly south-eastward, and equatorward in autumn-winter. This pattern is not clear in the (single) multiyear current time-series on the shelf that was available before the present study, which rather displays large seasonal and inter-annual fluctuations (see Figure 5 in Criado-Aldeanueva et al., 2009). Besides, our observations indicate that CCCs occur ~42% of the time, with no significant variations between summer and winter, and were generally associated with poleward rather than equatorward wind in the basin (Figure 9). To detail this distribution, occurrences of CCCs in July, August, November and December are reported in Table 3 on a yearly basis. During these months, the open sea water circulation is the strongest and coastal flow predominance should be the most pronounced (Criado-Aldeanueva et al., 2009). However, our data indicate that equatorward flows rather than CCCs generally prevailed in July-August, with the exception of August 2010. In November-

December, equatorward flows were only predominant in 2008, although the number of observations for each month is highly variable. These observations confirm the seasonal and inter-annual fluctuations of the coastal circulation, rather than poleward flow predominance in summer, at least at the mooring site. Hence, the presence of a seasonal cyclonic cell on the shelf of the eastern GoC is not supported by our dataset. Nevertheless, as noted by Criado-Aldeanueva et al. (2009), longer time-series are required to establish a definitive conclusion. Concurrent observations along the inner shelf are also desirable to establish the spatial variations of the coastal circulation. For example, observations off the Oregon coast have indicated that poleward flow patterns are significantly affected by shelf width variations (Kosro, 2005).

5.3. Inversions in response to wind stress alone

Water circulation is driven by wind in the GoC, and it is expected that wind has a major effect on the patterns of CCCs. This is well-illustrated with the broad correspondence observed between poleward flow and wind (Figure 9). It is also interesting to note that the correspondence among the alongshore wind time series is reasonably consistent as shown in Figure 10 and plate 1 from supplementary material. Westward winter storms clearly affect the intensity and duration of CCCs (e.g., November 2010 and November 2013 in Figure 3; Figure 4). However, despite some episodic good correspondences between poleward flow and wind (e.g., Figure 10a, b), numerous mismatch periods can be found (Figures 9 and 10c, d; see also the examples provided as supplementary material). In addition, the general patterns of CCCs do not support that they result directly from wind stress action alone. For example, the percentage of time with CCCs is similar in summer and winter (about 40%), while poleward winds are comparatively largely predominant in winter (compare Figures 2b and 2c). Likewise, maximum CCC velocities are as high in summer as in winter despite of lower wind conditions. In particular, the largest poleward flow velocity was associated with mild alongshore wind stress (< 0.03 N m^{-2}; see August 2010 in Figure 3; see also July 2008 for a similar example of weak wind associated with large CCC velocity). Likewise, the strongest poleward wind events of the time series do not correspond to particularly large CCC velocities (e.g., see the storms occurring in November 2008, at the end of Deployment 2, in Figure 3). Wind action alone also fails to explain why inversions frequently start near the bed rather than near the surface (as exemplified with an arrow in Figure 8a). Furthermore, lags between CCC and westward wind indicate that alongshore flows reverse more easily from equatorward to poleward than the opposite, in concordance with a relaxation process: the development of equatorward flows requires upwelling-favourable wind to blow for some time, while CCCs only require weak winds. This lag was also noted in the SST signal along the Californian coast, where warm water arrives at the beginning of wind relaxation periods but remains for some time after the upwelling wind resumed (Largier et al., 1993; Mace and Morgan, 2006; Melton et al., 2009; Send et al., 1987; Wing et al., 1995).

To examine intermittent linkages between alongshore wind stress and currents at various time scales and periods, the time-series were expanded in time-frequency space with a Cross Wavelet Transform (XWT) analysis (Grinsted et al., 2004). A Paul mother wavelet was used because it is expected to provide a better temporal resolution and thus to identify isolated events (such as sporadic inversions in the alongshore current direction) more accurately than other wavelets (De Moortel et al., 2004). The cross-wavelet power spectrum was calculated from the XWT results in order to estimate the covariance between each pair of time series as a function of frequency (Figure 13). The statistical significant level (95%) was estimated using Monte Carlo methods. The colour contours denote cross wavelet power (i.e., the covariance of the two time series) and the arrows designate their phase relationship (in-phase pointing right and out of phase pointing left). The thin black line delimits the cone of influence in which edge effects become significant (Grinsted et al., 2004). The highest wavelet power between alongshore wind stress and currents (both poleward and equatorward) is found in the band period 8-32 days, suggesting that the circulation at the mooring site is mainly forced by large-scale rather than local wind conditions. In agreement, previous studies at the GoC have suggested a strong control of large-scale atmospheric pressure systems on the seasonal inner-shelf (Sánchez et al., 2006) and offshore (Machín et al., 2006) circulations. Of particular interest for the present study, Sánchez et al. (2006) have indicated that alongshore currents near the mooring site are better correlated with wind at the West coast than with the local one. This pattern was also observed in other shelves where the local wind is relatively weak such as the SBC (Hickey et al., 2003). It should be noted, however, that in other upwelling regions (California, Peru, Oregon) the 8-32 days band period also corresponds to coastal trapped waves (CTW) produced by drastic changes in the large scale wind conditions (e.g., Battisti and Hickey, 1984; Camayo and Campos, 2006). In detail, our results indicate that CCCs with high common power was mostly associated with an in-phase relationship (arrows pointing to the right), although sometimes wind was leading currents (arrows pointing down; see the examples outlined with green boxes in Figure 13). For large CCC velocities, the cross-wavelet power often extends to shorter periods forming peaks (see the examples outlined with white boxes in Figure 13), suggesting that CCCs are more reactive than equatorward flows to local (i.e., short period) alongshore wind. Note however that the corresponding phase relationship was highly inconstant (e.g., see the variable arrows' direction in the white boxes of Figure 13). As a summary, the coastal water circulation seems to be largely controlled by wind that operates at a (8-32 days) band period which is characteristic of wind-induced current fluctuations in the Iberian upwelling system. The relationship between the short period alongshore wind stress and CCCs was not always clear, indicating that even though local alongshore wind is capable of affecting CCC patterns, it is not their main driving mechanism.

5.4.   Relaxation events

The observations provided in the previous section show that the action of wind alone generally fails to account for the development of CCCs, whatever a local or basin-scale wind source is considered. In some cases (see 22nd of May 2014 in Plate 1), inversions occurred in a context of decreasing (equatorward) alongshore wind intensity, in concordance with a relaxation process. However, this correspondence was not always observed. As striking examples, inversions occurred while equatorward wind was intensifying at all sources on the 30th of October 2010 and 12th of July 2014 (Plate 1). It seems therefore that, relaxation or not, alongshore local (or basin-scale) wind poorly controls the development of CCCs.

The coherency and cross-correlation (at lag 0) of the alongshore flow and wind rotated in 18 sectors of 10° was then computed to identify which wind direction is best correlated with the alongshore circulation (Figure 14). Both the largest coherency (at the 2-5 days period band) and the largest cross-correlation correspond to wind oriented SE-NW. Similar results were obtained when a lag was introduced in the cross-correlation (with the best correlation for a 16 h lag). Wind blows predominantly south-eastward but rarely north-westward in the region, particularly in summer (Figure 2). Hence, the coherency and cross-correlation results indicate that the alongshore circulation is mainly forced by south-eastward wind in the GoC. South-eastward wind proceeds from the rotation around CSV of upwelling-favourable southward wind at the West coast, which ultimately controls the inner-shelf circulation in the GoC (Sánchez et al., 2006). This view is consistent with the XWT results indicating that the coastal circulation at the studied site is mainly controlled by wind operating at the scale of the upwelling system (such as southward wind at the West coast and south-eastward wind at the South coast). Such correspondence between CCCs and upwelling-favourable wind (at the scale of the system) points out towards a relaxation process.

In the frame of the CODE experiment, Huyer and Kosro (1987) performed a linear regression analysis between alongshore wind and flow to examine the current direction tendency in the absence of wind (zero intercept of the regression), as an indication of the flow response to relaxation. This approach was applied to the present dataset considering alongshore current and the best correlated SE-NW rotated wind (see Figure 14b). Considering a 16 h lag, the results indicate that under no wind conditions the flow tends to be poleward (~1 cm s^{-1}) in summer and equatorward (~3 cm s^{-1}) in winter. Similar tendencies are obtained with a 0 lag and when storms (wind speed > 5 m s^{-1}) are discarded. Such flow behaviour is contrary to the shelf circulation scheme (cyclonic in summer, anticyclonic in winter) proposed in previous studies (Criado-Aldeanueva et al., 2009; García-Lafuente et al., 2006; see Section 5.2). In summer, this behaviour is concordant with the development of CCCs in response to the unbalance of an APG during the relaxation of upwelling-favourable wind (while in winter, the APG might not be predominant compared to other processes).

The points discussed above strongly suggest that the observed linkage between CCCs and (system-scale) upwelling favourable winds in the eastern GoC result from a relaxation process. It is not the objective of the present report to address the dynamics of such

process. Nevertheless, it is verified whether realistic relaxation events that match CCC periods can be defined considering northwest-southeast wind at Cadiz buoy. Following Melton et al. (2009), thresholds based on wind intensity and duration were considered to define wind relaxation events. The relaxation begins at a time Tb when (south-eastward) wind velocity drops below a threshold value of 3 m s^{-1} (see the example in Figure 15). Additionally, it is required that wind blows above this threshold during at least 70% of the 2 days preceding Tb, and below the threshold during more than 50% of the 2 days following Tb. Successive Tb were separated by at least 1.5 days to be retained. The end of relaxation (Te) is defined when wind is above a threshold of 4 m s^{-1} for at least 36 hours. Note that with a threshold of 3 m s^{-1}, as defined for Tb, CCCs would reverse largely after Te. Distinct threshold velocities for Tb and Te are consistent with our observations (although for alongshore wind) that poleward flows are more difficult to reverse than equatorward flows. A 5-day relaxation period defined with the above criteria is presented in Figure 15. In this example, the development of a poleward flow corresponds closely to the relaxation window, and its intensity is somewhat modulated by the wind speed.

Overall, the defined periods of wind relaxation occur all year-round and match well (91%) the periods of poleward flow (Figure 9). Few of these periods are not associated with relaxation, such as when CCCs are weak (< 0.1 m s^{-1}) or when relaxations could not be defined at the start and end of deployments. Only one strong CCC event (9th of November 2008) corresponded to a winter storm that was not recognised as a relaxation event by the procedure. The selected criteria for the definition of relaxation events are similar to those proposed at the SBC (see Melton et al., 2009). The main difference is that the wind speed thresholds are lower in our case, in particular at the start of relaxation (3 m s^{-1} in the GoC, against 5 m s^{-1} in the SBC). However, the thresholds along the California coast were defined based on wind at the west coast, where wind conditions are stronger than at the south coast. Finally, the proposed relaxation criteria for the GoC are plausible and give reasonable results; they are however subjective and should be based on objective identification procedures to be definitive.

6. Conclusions

This study has characterised, for the first time, the main patterns of CCCs based on a multiyear time series of current observations on the inner shelf of the GoC. The coastal circulation is mainly alongshore and barotropic. Poleward flows, up to 0.4 m s^{-1}, develop all year-round but are not associated with warmer water in winter. During the upwelling season, CCCs control the occurrence of warm water, increasing the vertical stratification, with faster flows leading to larger temperature increases. The mean duration of CCC events was 3 days, even though long events lasting up to 15 days were observed. Peak velocity and duration are well-correlated for CCC events less than 5 days-long. Inversions often start near the bed and are accompanied with the development of a 2-layer cross-shore flow often typical of downwelling conditions. Such cross-shore water exchanges during poleward flows

may affect the availability of nutrients at near-shore areas should be addressed in future studies.

In total, about 1 inversion per week was observed, corresponding to the occurrence of CCCs during as much as 40% of the time, with no seasonal trend. Thus, the dynamics of the studied coastal area is dominated by the temporary development of CCCs all year-round. Although longer, the periods of the annual cycle governed by the Ekman mechanism, inducing the upwelling of cold water along the coast and the associated eastward geostrophic flow, are comparable to those governed by the CCCs. Regarding this fact, it is excessive to assume the region as an upwelling system, defined as a system where upwelling prevails during at least a substantial part of the year (in some places permanently). Contrarily to the African boundary of the CCUS, the coupling between atmospheric forcing, ocean circulation, biogeochemical cycling and food web dynamics attributed to the Ekman dynamics may not fully develop in the northern margin of the GoC. The latter is rather a system where upwelling events do occur during the western Iberian upwelling season.

At the local or basin scales, poleward winds clearly affect the pattern (duration, velocity) of CCCs, particularly during winter storms. However, the general patterns of CCCs do not reproduce the seasonal patterns of alongshore wind stress. This shows that CCCs are not produced as a result of the sole action of wind stress, as demonstrated by the mismatch between alongshore flow and wind, even when various wind sources are considered. In contrast, wavelet analysis indicates that CCCs are best correlated with large-scale wind occurring in a band period characteristic of the upwelling system. Concordantly, alongshore currents exhibit largest coherency and cross-correlation with south-eastward wind which proceeds from the counter clockwise rotation around CSV of upwelling favourable southward wind at the West coast. The inner-shelf circulation at the GoC seems therefore to be largely controlled by large-scale wind conditions, as proposed in previous studies (Sánchez et al., 2006). Overall, our results support that the unbalance of an APG due to the relaxation of large-scale upwelling-favourable wind drives the development of CCCs in the eastern GoC. Considering south-eastward wind, realistic thresholds can be defined for the identification of relaxation periods that include most of the observed periods with poleward flow. Future work should aim at identifying the main process that produce the APG, and at assessing the contribution of CTW.

Acknowledgments

References

Battisti, D.S., and Hickey, B.M., 1984, Application of remote wind forced coastal trapped wave theory to the Oregon and Washington coasts: Journal of Physical Oceanography, v. 14, p. 887-903.

Camayo, R., and Campos, E.J.D., 2006, Application of wavelet transform in the study of coastal trapped waves off the west coast of South America: Geophysical Research Letters, v. 33, p. L22601.

Criado-Aldeanueva, F., García-Lafuente, J., Navarro, G., and Ruiz, J., 2009, Seasonal and interannual variability of the surface circulation in the eastern Gulf of Cadiz (SW Iberia): Journal of Geophysical Research, v. 114.

Criado-Aldeanueva, F., García-Lafuente, J., Vargas, J.M., Del Río, J., Sánchez, A., Delgado, J., and Sánchez, J.C., 2006, Wind induced variability of hydrographic features and water masses distribution in the Gulf of Cadiz (SW Iberia) from in situ data: Journal of Marine Systems, v. 63, p. 130-140.

De Moortel, I., Munday, S.A., and Hood, A.W., 2004, Wavelet analysis: The effect of varying basic wavelet parameters: Solar Physics, v. 222, p. 203-228.

Dever, E.P., 2004, Objective maps of near-surface flow states near Point Conception, California: Journal of Physical Oceanography, v. 34, p. 444-461.

Dudas, S.E., Grantham, B.A., Krinincich, A.R., Menge, B.A., Lubchenco, J., and Barth, J.A., 2008, Current reversals as determinants of intertidal recruitment on the central Oregon coast: ICES Journal of Marine Science, v. 66, p. 396-407.

Fawcett, A.L., Pitcher, G.C., and Shillington, F.A., 2008, Nearshore currents on the southern Namaqua shelf of the Benguela upwelling system: Continental Shelf Research, v. 28, p. 1026-1039.

Fiúza, A.F.G., 1983, Upwelling Patterns off Portugal: New York, Plenum.

Fiúza, A.F.G., Macedo, M.E., and Guerreiro, M.R., 1982, Climatological space and time variation of the Portuguese coastal upwelling: Oceanologica Acta, v. 5, p. 31- 40.

Folkard, A.W., Davis, P.A., Fiúza, A.F.G., and Ambar, I., 1997, Remotely sensed se surface thermal patterns in the Gulf of Cádiz and the Strait of Gibraltar: variability,

correlations, and relationships with the surface wind field: Journal of Geophysical Research, v. 102, p. 5669-5683.

Gan, J., and Allen, J.S., 2002, A modeling study of shelf circulation off northern California in the region of the Coastal Ocean Dynamics Experiment: Response to relaxation of upwelling winds: Journal of Geophysical Research: Oceans, v. 107, p. 3123.

García-Lafuente, J., Delgado, J., Criado-Aldeanueva, F., Bruno, M., del Río, J., and Miguel Vargas, J., 2006, Water mass circulation on the continental shelf of the Gulf of Cádiz: Deep Sea Research Part II: Topical Studies in Oceanography, v. 53, p. 1182-1197.

Garel, E., and Ferreira, Ó., 2013, Fortnightly Changes in Water Transport Direction Across the Mouth of a Narrow Estuary: Estuaries and coasts, v. 36, p. 286-299.

Grinsted, A., Moore, J.C., and Jevrejeva, S., 2004, Application of the cross wavelet transform and wavelet coherence to geophysical time series: Nonlinear Processes in Geophysics, v. 11, p. 561-566.

Harms, S., and Winant, C.D., 1998, Characteristic patterns of the circulation in the Santa Barbara Channel: Journal of Geophysical Research: Oceans, v. 103, p. 3041-3065.

Haynes, R., Barton, E.D., and Pilling, I., 1993, Development, persistence, and variability of upwelling filaments off the Atlantic coast of the Iberian Peninsula: Journal of Geophysical Research, v. 98, p. 22,681– 22,692.

Hickey, B.M., Dobbins, E.L., and Allen, S.E., 2003, Local and remote forcing of currents and temperature in the central Southern California Bight: Journal of Geophysical Research: Oceans, v. 108, p. n/a-n/a.

Huyer, A., and Kosro, P., 1987, Mesoscale surveys over the shelf and slope in the upwelling region near Point Arena, California: Journal of Geophysical Research, v. 92, p. 1655-1681.

Kosro, P.M., 2005, On the spatial structure of coastal circulation off Newport, Oregon, during spring and summer 2001 in a region of varying shelf width: Journal of Geophysical Research: Oceans, v. 110, p. n/a-n/a.

Large, W.G., and Pond, S., 1981, Open ocean momentum flux measurements in moderate to strong winds: Journal of physical oceanography, v. 11, p. 324-336.

Largier, J.L., Magnell, B.A., and Winant, C.D., 1993, Subtidal circulation over the northern California shelf: Journal of Geophysical Research, v. 98, p. 18,147-18,179.

Lentz, S.J., and Chapman, D.C., 1989, Seasonal differences in the current and temperature variability over the northern California shelf during the Coastal Ocean Dynamics Experiment: Journal of Geophysical Research, v. 94.

Lobo, F.J., Sánchez, R., González, R., Dias, J.M.A., Hernández-Molina, F.J., Fernández-Salas, L.M., Díaz del Río, V., and Mendes, I., 2004, Contrasting styles of the Holocene

highstand sedimentation and sediment dispersal systems in the northern shelf of the Gulf of Cadiz: Continental Shelf Research, v. 24, p. 461-482.

Mace, A.J., and Morgan, S.G., 2006, Biological and physical coupling in the lee of a small headland: Contrasting transport mechanisms for crab larvae in an upwelling region: Marine Ecology Progress Series, v. 324, p. 185-196.

Machín, F., Pelegrí, J.L., Marrero-Díaz, A., Laiz, I., and Ratsimandresy, A.W., 2006, Near-surface circulation in the southern Gulf of Cádiz: Deep Sea Research Part II: Topical Studies in Oceanography, v. 53, p. 1161-1181.

Mauritzen, C., Morel, Y., and Paillet, J., 2001, On the influence of Mediterranean water on the central waters of the North Atlantic Ocean: Deep-Sea Research I, v. 48, p. 347-381.

Melton, C., Washburn, L., and Gotschalk, C., 2009, Wind relaxations and poleward flow events in a coastal upwelling system on the central California coast: Journal of Geophysical Research - Oceans, v. 114.

Mittelstaedt, E., 1991, The ocean boundary along the Northwest African coast: Circulation and oceanographic properties at the sea surface: Progress in Oceanography, v. 26, p. 307-355.

Navarro, G., and Ruiz, J., 2006, Spatial and temporal variability of phytoplankton in the Gulf of Cádiz through remote sensing images: Deep Sea Research II, v. 53, p. 1241-1260.

Pelegrí, J.L., Arístegui, J., Cana, L., González-Dávila, M., Hernández-Guerra, A., Hernández-León, S., Marrero-Díaz, A., Montero, M.F., Sangrà, P., and Santana-Casiano, M., 2005a, Coupling between the open ocean and the coastal upwelling region off Northwest Africa: Water recirculation and offshore pumping of organic matter: Journal of Marine Systems, v. 54, p. 3-37.

Pelegrí, J.L., Marreo-Díaz, A., Ratsimandresy, A.W., Antoranz, A., Cisneros-Aguirre, J., Gordo, C., Grisolía, D., Hernández-Guerra, A., Laiz, I., Martínez, A., G.Parrilla, Pérez-Rodríguez, P., Rodríguez-Santana, A., and Sangrà, P., 2005b, Hydrographic cruises off Northwest Africa: The Canary Current and the Cape Ghir region: Journal of Marine Systems, v. 54, p. 39-63.

Peliz, Á., Santos, A.M.P., Oliveira, P.B., and Dubert, J., 2004, Extreme cross-shelf transport induced by eddy interactions southwest of Iberia in winter 2001: Geophysical Research Letters, v. 31, p. 1-4.

Peliz, A.J., and Fiuza, A.F.G., 1999, Temporal and spatial variability of CZCS-derived phytoplankton pigment concentrations off the western Iberian Peninsula: International Journal of Remote Sensing, v. 20, p. 1363-1403.

Relvas, P., and Barton, E.D., 2002, Mesoscale patterns in the Cape Sãᵒ Vicente (Iberian Peninsula) upwelling region: Journal of Geophysical Research, v. 107.

Sánchez, R.F., Mason, E., Relvas, P., da Silva, A.J., and Peliz, Á., 2006, On the inner-shelf circulation in the northern Gulf of Cádiz, southern Portuguese shelf: Deep Sea Research Part II: Topical Studies in Oceanography, v. 53, p. 1198-1218.

Sánchez, R.F., and Relvas, P., 2003, Spring–summer climatological circulation in the upper layer in the region of Cape St. Vincent, Southwest Portugal: ICES Journal of Marine Science, v. 60, p. 1232-1250.

Send, U., Beardsley, R.C., and Winant, C.D., 1987, Relaxation from upwelling in the Coastal Ocean Dynamics Experiment: Journal of Geophysical Research: Oceans, v. 92, p. 1683-1698.

Stacey, M.T., Burau, J.R., and Monismith, S.G., 2001, Creation of residual flows in a partially stratified estuary: Journal of Geophysical Research, v. 106, p. 17013-17043.

Teles-Machado, A., Peliz, Á., Dubert, J., and Sánchez, R.F., 2007, On the onset of the Gulf of Cadiz Coastal Countercurrent: Geophysical Research Letters, v. 34, p. L12601.

Vargas, J.M., García-Lafuente, J., Delgado, J., and Criado, F., 2003, Seasonal and wind-induced variability of Sea Surface Temperature patterns in the Gulf of Cádiz: Journal of Marine Systems, v. 38, p. 205-219.

Washburn, L., Fewings, M.R., Melton, C., and Gotschalk, C., 2011, The propagating response of coastal circulation due to wind relaxations along the central California coast: Journal of Geophysical Research: Oceans, v. 116, p. C12028.

Washburn, L., and McPhee-Shaw, E., 2013, Coastal transport processes affecting inner-shelf ecosystems in the California Current System: Oceanography, v. 26, p. 34-43.

Wilson, J.R., Broitman, B.R., Caselle, J.E., and Wendt, D.E., 2008, Recruitment of coastal fishes and oceanographic variability in central California: Estuarine, Coastal and Shelf Science, v. 79, p. 483 - 490.

Winant, C., Alden, D., Dever, E., Edwards, K., and Hendershott, M., 1999, Near-surface trajectories off central and southern California: Journal of Geophysical Research, v. 104, p. 15,713-15,726.

Winant, C.D., Beardsley, R.C., and Davis, R.E., 1987, Moored wind, temperature, and current observations made during the Coastal Ocean Dynamics Experiments 1 and 2 over the northern California continental shelf and upper slope: Journal of Geophysical Research, v. 92, p. 1569- 1604.

Winant, C.D., Dever, E.P., and Hendershott, M.C., 2003, Characteristic patterns of shelf circulation at the boundary between central and southern California: Journal of Geophysical Research, v. 108, p. 3021.

Wing, S.R., Botsford, L.W., Largier, J.L., and Morgan, L.E., 1995, Spatial structure of relaxation events and crab settlement in the northern California upwelling system: Marine Ecology Progress Series, v. 128, p. 199–211.

Woodson, C.B., Washburn, L., Barth, J.A., Hoover, D.J., Kirincich, A.R., McManus, M.A., Ryan, J.P., and Tyburczy, J., 2009, Northern Monterey Bay upwelling shadow front: Observations of a coastally and surface trapped buoyant plume: Journal of Geophysical Research, v. 114, p. C12013.

Wooster, W.S., Bakun, A., and McLain, D.R., 1976, The seasonal upwelling cycle along the eastern boundary of the North Atlantic: Journal of Marine Research, v. 34, p. 131-141.

Table captions

Table 1. ADCP deployment periods.

Table 2. Duration of ADCP observations (in hours, hr) and patterns of coastal counter-currents (CCCs) for each month and for all the dataset: CCC occurrence (percentage of time with poleward flow); monthly mean (and total, in brackets) number of current inversions; monthly mean (and maximum, in brackets) duration of CCC events (in days). No data were recorded in March.

Table 3. Percentage of occurrence of poleward flows in July, August, November and December, per year. The number of hourly observations for each month is indicated in brackets ("-": no observation).

Figure captions

Figure 1. Localisation of the ADCP mooring (red point) and wind sources used in this study (green stars). ETOPO1 bathymetric contours (-100m, -500m and -1000m) are indicated. CSV: Cape St Vicente; CSM: Cape Santa Maria.

Figure 2. Wind roses of the concatenated observations represented with the oceanographic convention: (a) all data; (b) June-August; and (c) November-January.

Figure 3. (a) Depth averaged alongshore velocity (u_x, red line, positive equatorward, m s^{-1}); (b) depth averaged cross-shore velocity (u_y, green line, positive landward, m s^{-1}); (c) near-bed temperature (black line, °C); and, (d) alongshore wind stress at Cadiz buoy (τw_x, blue line, N.m^{-2}) during the 7 ADCP deployment periods. The tick interval along the x-axis is 10 days, but note that the dates are not continuous: for visualisation, the 7 continuous time-series are concatenated chronologically and distinguished with grey and white background colours (see also the labels on top of the graph).

Figure 4. Monthly patterns of CCC events: (a) duration o; (b) peak velocity. The red lines are monthly-averaged.

Figure 5. Maximum peak velocity of CCC events Vs duration. Summer (June-August) and winter (November-January) months are represented with blue and red circles, respectively.

Figure 6. Histogram of temperature data considering the entire time-series (blue), the periods with CCCs (green), and the periods with CCCs during the upwelling season (May-October; brown).

Figure 7. Peak alongshore velocity (u_{max}, m s^{-1}) and associated temperature increase (dT, °C) during CCC events in summer (June-August). The red line indicates the linear fit (r = 0.89).

Figure 8. Vertical structure of the (a) alongshore flow (m s^{-1}) and (b) cross-shore flow at the mooring site. (c) Temperature measured by the thermistors near the surface (7 m depth, blue line), at mid depth (13 m depth, red line) and near the bed (18 m depth, black line), and by the bottom-mounted ADCP (21 m, green line). The arrows and vertical dashed lines indicate an example of baroclinic alongshore flow at current inversion (see also Figures 11g and 12h).

Figure 9. Comparison of periods with CCC (red) and periods with westward alongshore wind from various sources (Hirlam: light blue; ASCAT: grey; Tavira: green; Cadiz buoy: dark blue) and with the relaxation periods (black). Wind-CCC relations are described in Section 4.3., while relaxation events are defined and compared with CCC in Section 5.4. The time series of each deployment are concatenated and separated with vertical lines (see also the labels on top of the graph). The percentage of time with poleward wind during poleward flow faster than 0.1 m s^{-1} is also indicated.

Figure 10. Examples where periods of poleward currents (upper row) and wind (lower row, with Tavira: blue; Cadiz: black; ASCAT: red; Hirlam: green) match in October 2008 (a) and November 2012 (b) and where they do not match in May 2008 (c) and January 2014 (d).

Figure 11. Energy (m^2.s^{-2}) of the near-bed PC1 (a) and PC2 (b) alongshore current components; Normalised velocity of the near-bed PC1 (c) and PC2 (d); Velocity (m s^{-1}) of the recorded alongshore currents (e). The grey areas indicate the main periods of poleward flow near the bed. The vertical dashed lines indicate the time of the examples of flow structure displayed on the right of the figure: 19th of August 2014 (f) and 7th of September 2014 (g). The latter example corresponds to the event annotated with arrows and dashed lines in Figure 8 and to Figure 12h.

Figure 12. Energy (m^2.s^{-2}) of the near-bed PC1 (a) and PC2 (b) cross-shore current components; Normalised velocity of the near-bed PC1 (c) and PC2 (d); Velocity (m s^{-1}) of the recorded depth-average cross-shore (e) and alongshore (f) flow. The grey areas indicate the periods of poleward flow. The vertical dashed lines indicate the time of the examples of flow structure displayed on the right of the figure: 20th of August 2014 (g) and 7th of September 2014 (h). The latter example corresponds to the event annotated with arrows and dashed lines in Figure 8 and to Figure 11g.

Figure 13. Cross wavelet transform analyses between the alongshore wind stress and (depth averaged) currents for each deployment. Arrows indicate the phase relationship between the 2 time-series, with in-phase pointing right and out of phase pointing left. White regions on both ends of the graphs indicate the "cone of influence", where edge effects become important. The negative alongshore current velocities are indicated on top of each graph (white line) to indicate the periods of poleward flow; the horizontal dashed line is -0.1 m s^{-1}. Green boxes exemplifies periods of CCC with high common wavelet power. White boxes exemplify the expansion of the common wavelet power from long to shorter periods during large CCC events. Note that the scale of the x- and y-axis varies for each deployment.

Figure 14. Magnitude of the squared coherence (a) and maximum cross-correlation at lag 0 (b) between the alongshore current and wind (Cadiz buoy) rotated per 10° sector. The wind direction is the direction the wind is blowing towards.

Figure 15. Example of a 5-day wind relaxation period as defined by Tb and Te described in the text. The alongshore current velocity is indicated in blue (m s^{-1}, left y-axis). Wind velocity rotated along the NW-SE direction is in green (right y-axis, m s^{-1}). **Supplementary Material**

Plate 1. Examples of the alongshore current and wind velocities (equatorward: positive; poleward negative) at times of poleward flows. Winds are from various sources: Tavira coastal station (blue); Cadiz offshore buoy (black); ASCAT remotely-sensed data (red); and Hirlam model outputs (green).
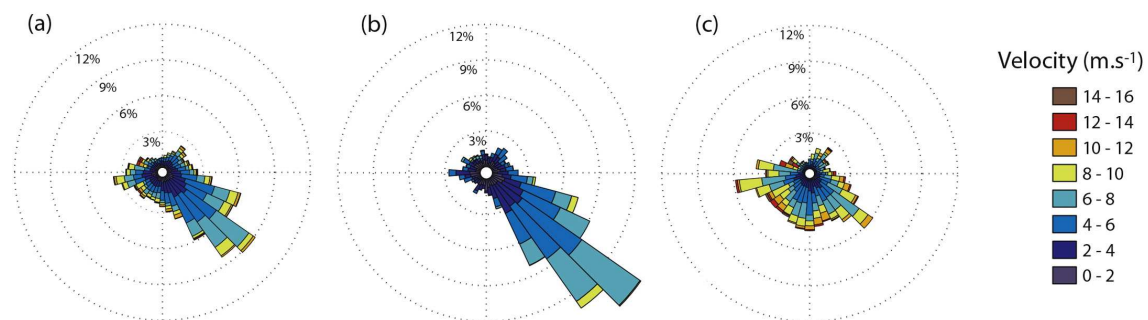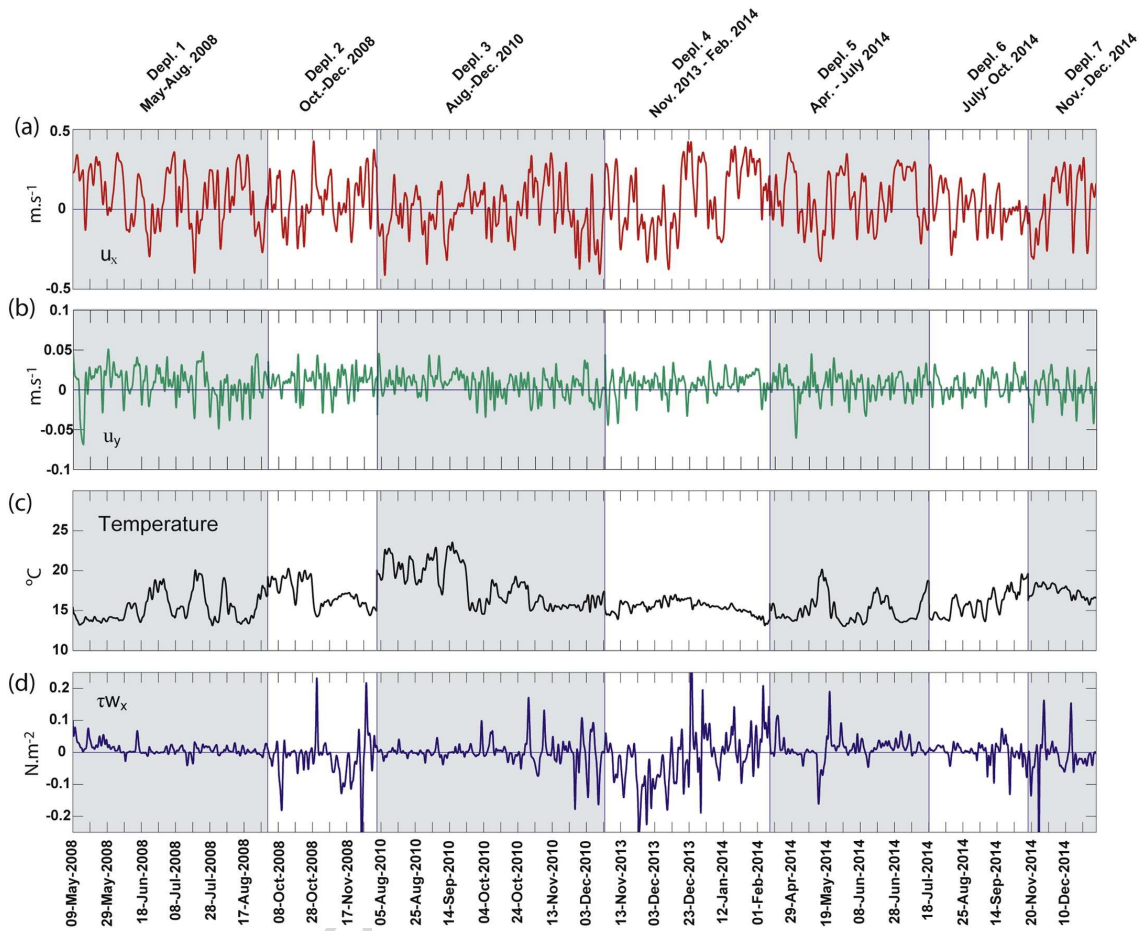
Figure 1

Figure 2

Depl. 1
May-Aug. 2008

Depl. 2
Oct.-Dec. 2008

Depl. 3
Aug.-Dec. 2010

Depl. 4
Nov. 2013 - Feb. 2014

Depl. 5
Apr. - July 2014

Depl. 6
July- Oct. 2014

Depl. 7
Nov.- Dec. 2014

(a)

$m.s^{-1}$

u_x

(b)

$m.s^{-1}$

u_y
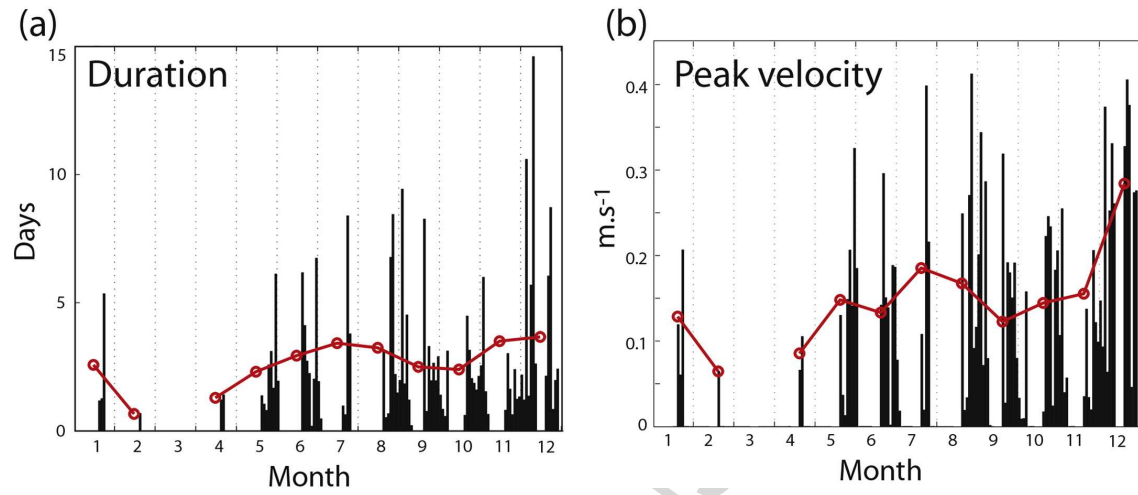
(c)

Temperature

°C

(d)

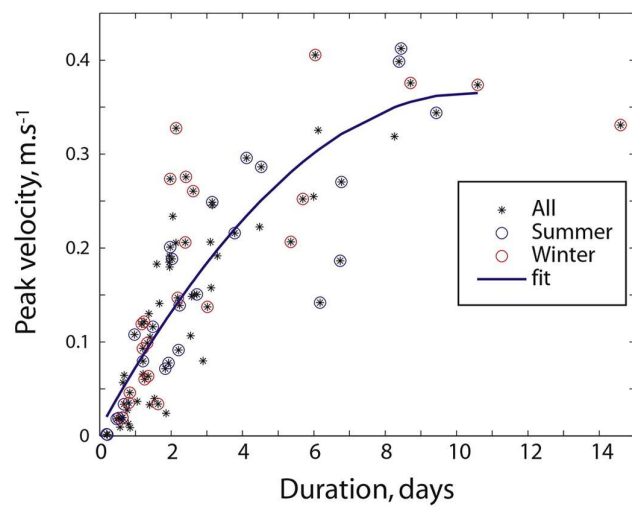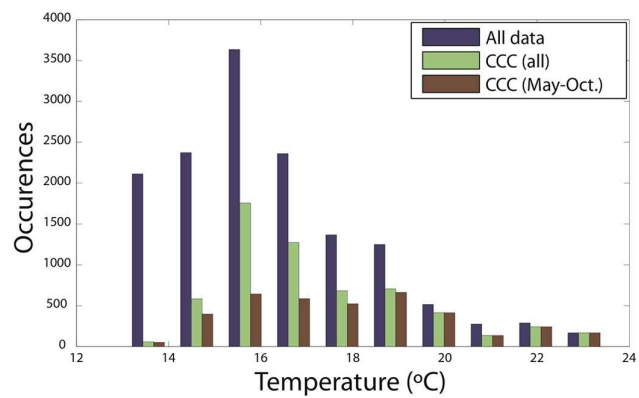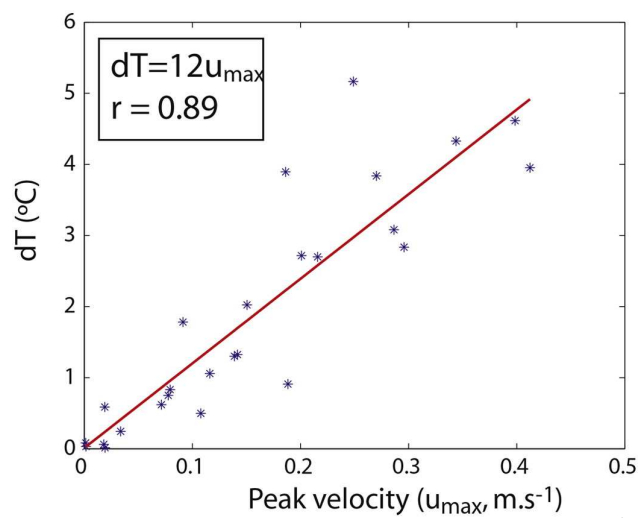τw_x

$N.m^{-2}$

Figure 3
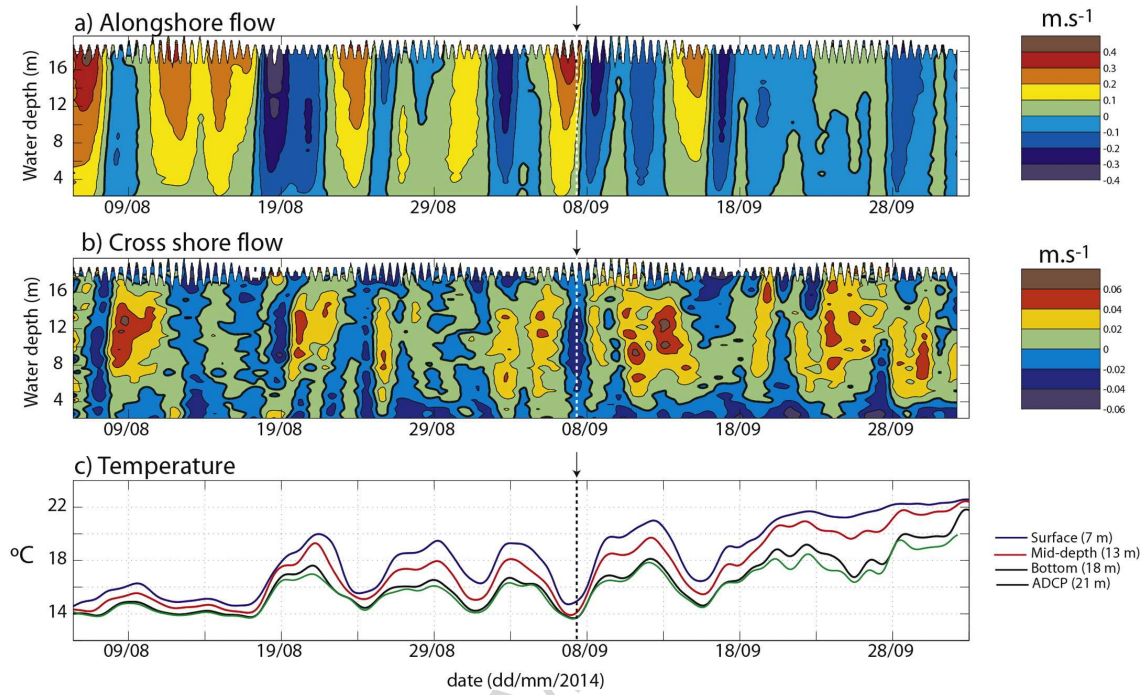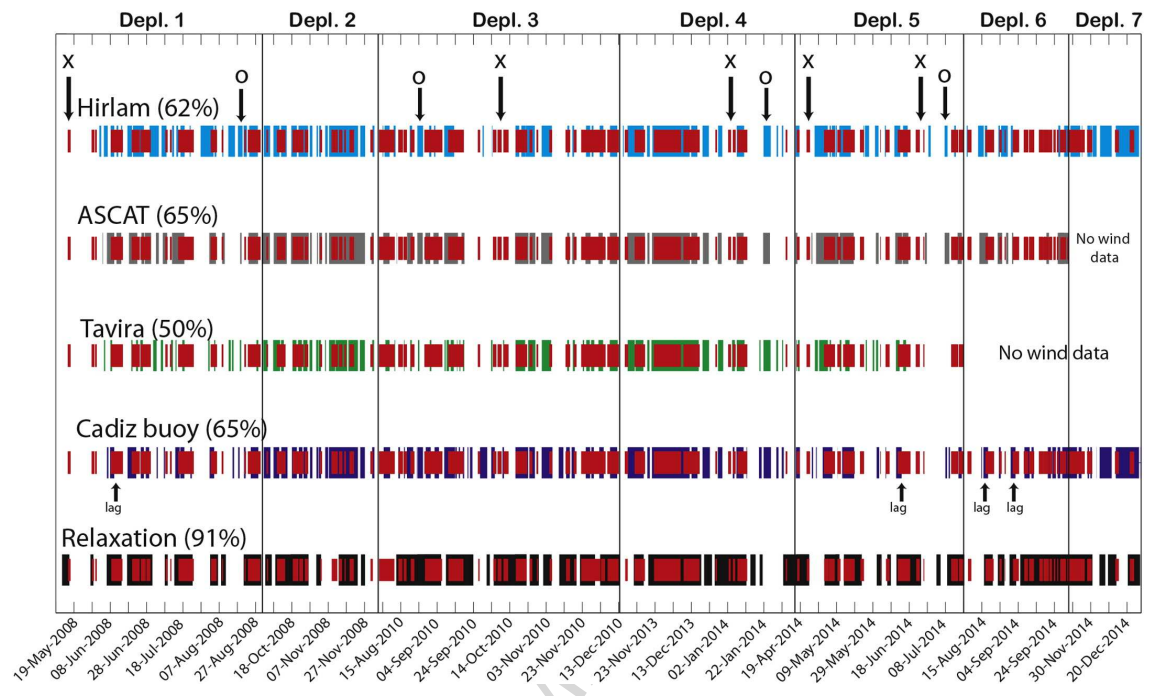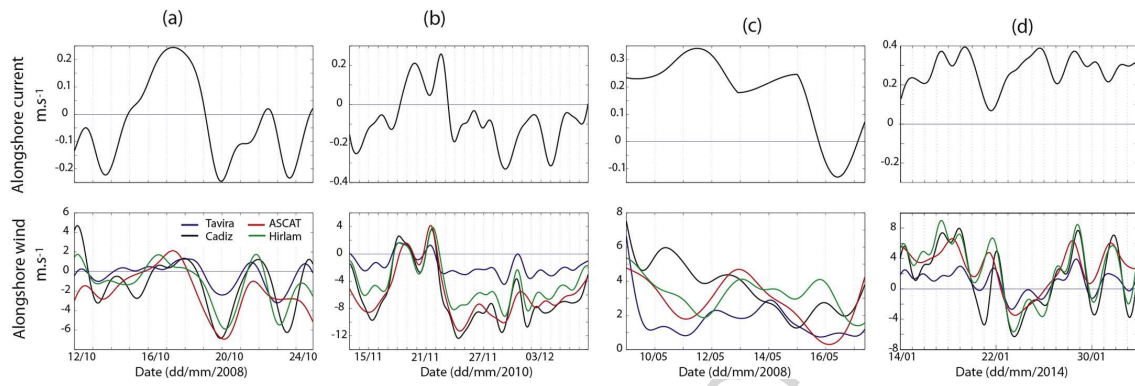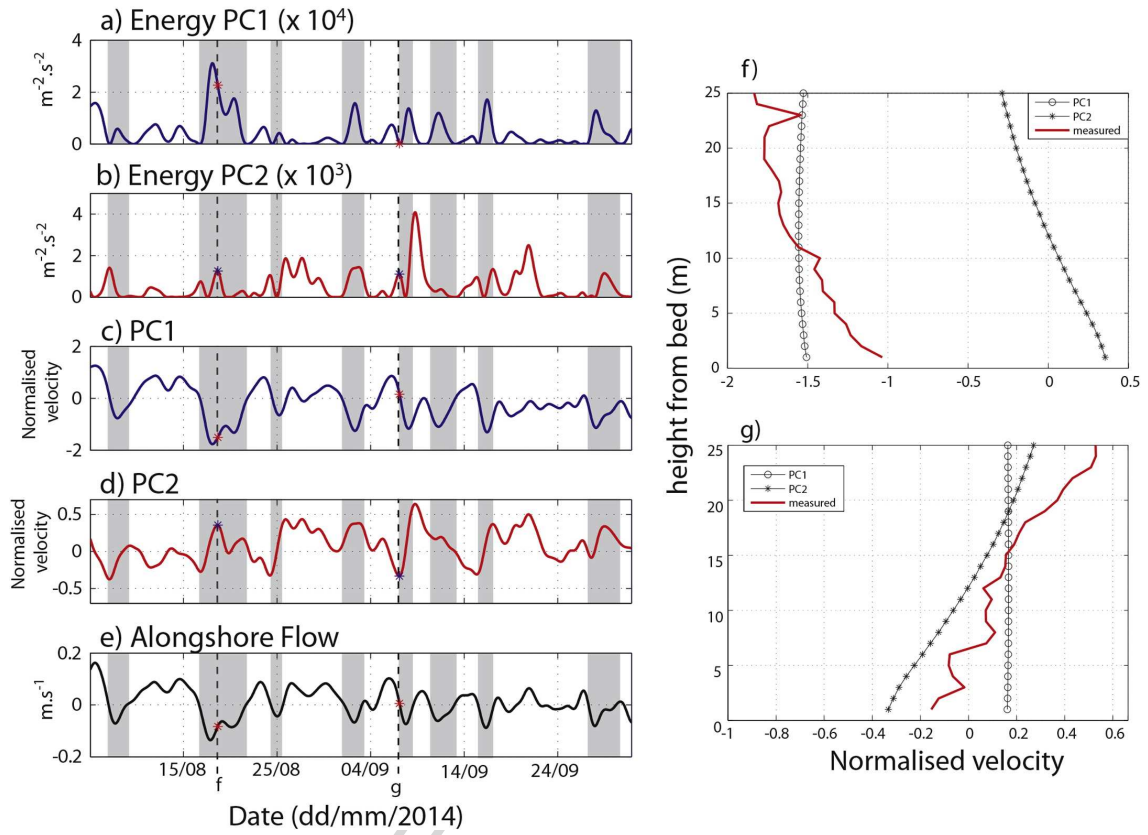
(a) Duration

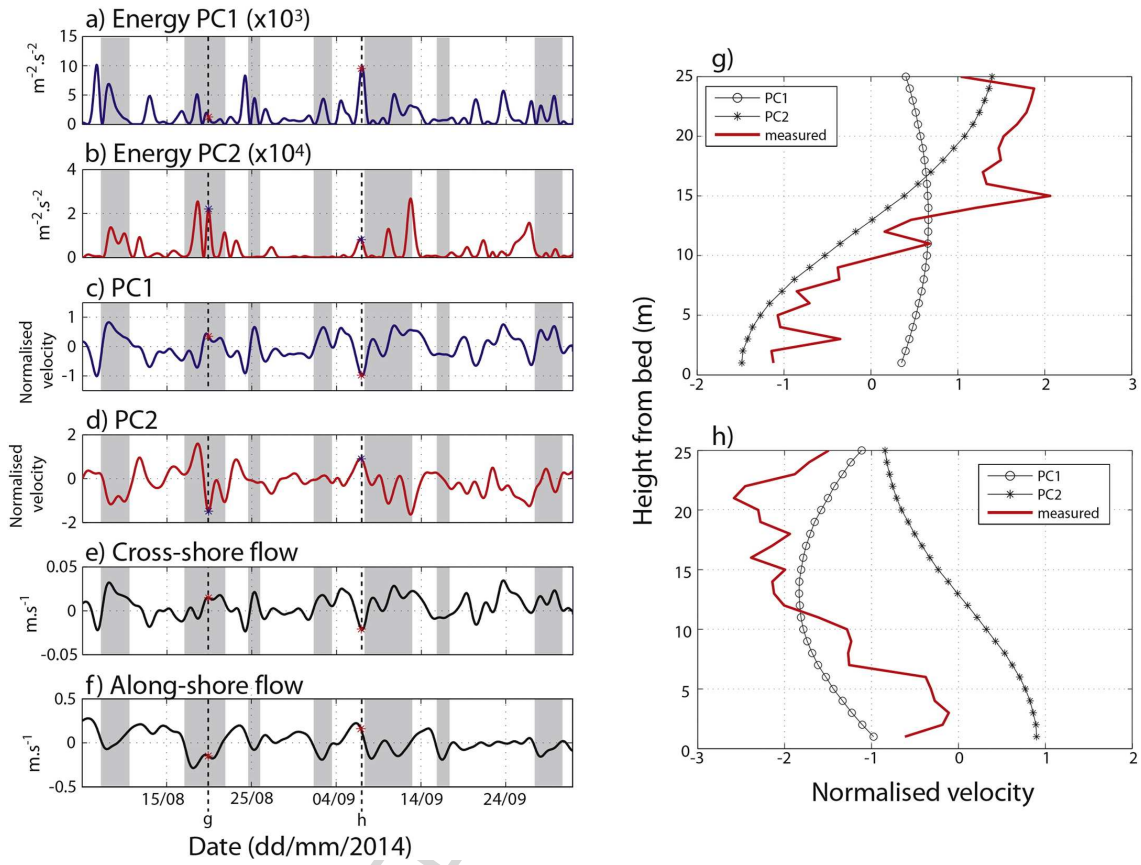(b) Peak velocity
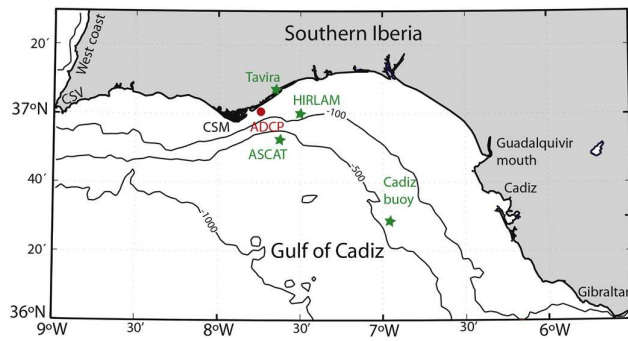
Figure 4

Figure 5

Figure 6

Figure 7

Figure 8

Figure 9

Figure 10

Figure 11

Figure 12

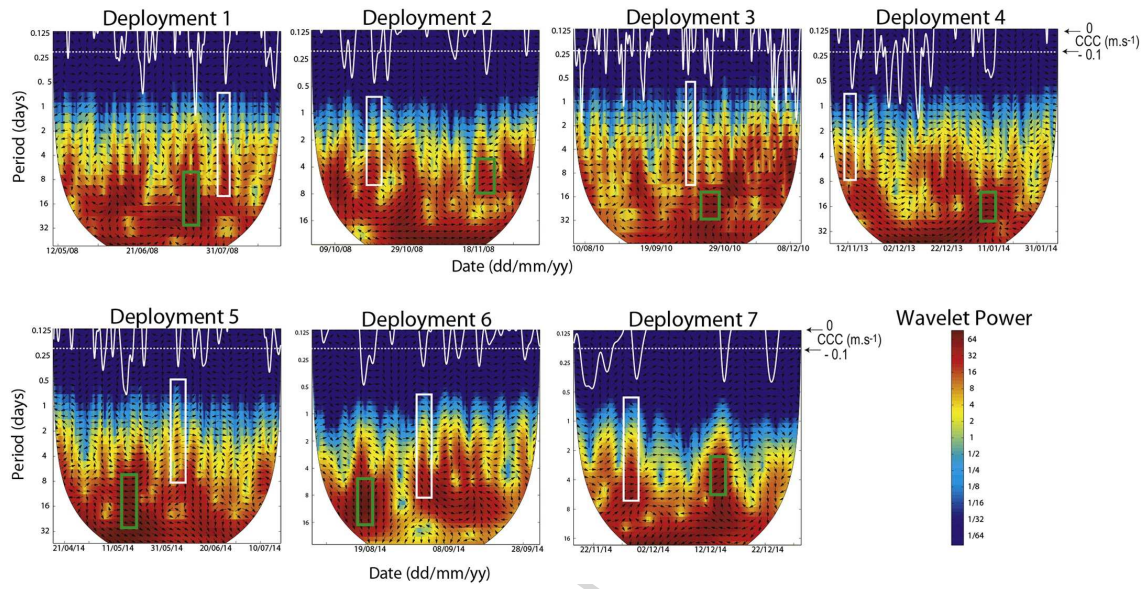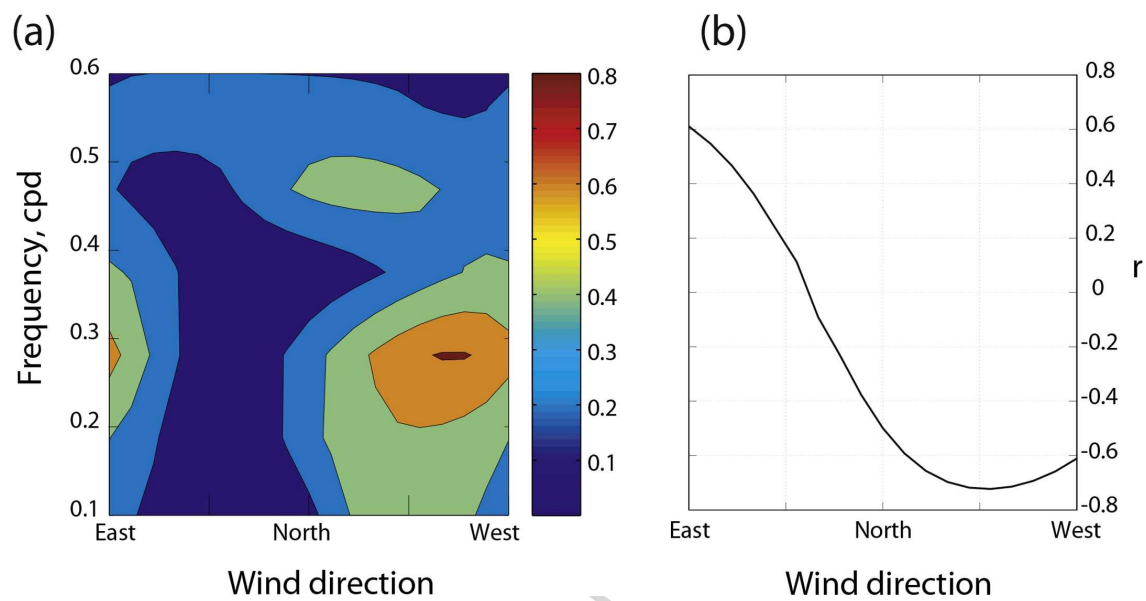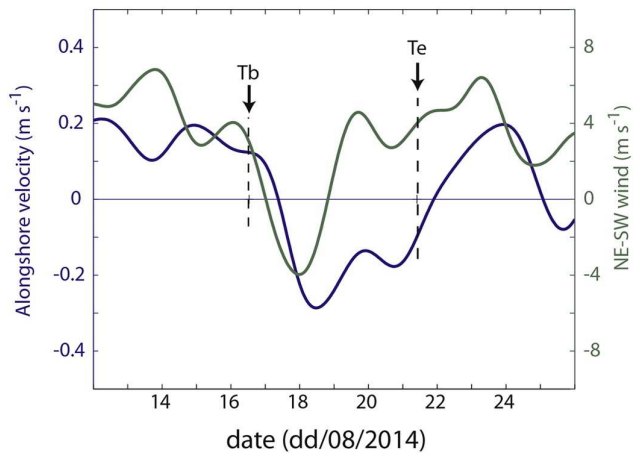Figure 13

(a)

(b)

Figure 14

Figure 15

Table 1

Deployment	Start	End	Duration (days)
1	09-May-2008	31-Aug-2008	114
2	02-Oct-2008	05-Dec-2008	64
3	03-Aug-2010	14-Dec-2010	133
4	04-Nov-2013	08-Feb-2014	96
5	16-Apr-2014	18-Jul-2014	93
6	05-Aug-2014	02-Oct- 2014	58
7	18-Nov-2014	28-Dec-2014	40

Table 2

	Jan.	Feb.	Apr.	May	Jun.	Jul.	Aug.	Sep.	Oct.	Nov.	Dec.	Winter	Summer	All data
Observations (hr)	744	190	351	1,282	1,440	1,160	2,056	1,440	1,483	2,377	1,823	4944	4656	14,346
CCC occurrence (%)	25	9	19	35	45	34	42	57	44	47	44	43	41	42
Monthly mean (total) number of inversions	2.9 (3)	3.8 (1)	4.1 (2)	4.5 (8)	4.5 (9)	2.5 (4)	4.5 (13)	5.5 (11)	5.3 (11)	4.2 (14)	2.4 (6)	3.3 (23)	4.0 (26)	4.1 (82)
Monthly mean (max) duration of inversion (days)	2.6 (5.4)	0.69 (0.69)	1.3 (1.4)	2.3 (6.1)	3 (6.7)	3.4 (8.4)	3.3 (9.4)	2.5 (8.3)	2.4 (6)	3.6 (14.6)	3.7 (8.7)	3.4 (14.6)	3.2 (9.4)	2.9 (14.6)

Table 3

Year	July	August	November	December
2008	32% (744)	37% (730)	28% (720)	30% (101)
2010	-	59% (687)	42% (720)	82% (322)
2013	-	-	55% (637)	53% (744)
2014	37% (416)	29% (639)	89% (300)	17% (656)

Plate 1